Cell Stem Cell
Article

Enhanced Telomere Rejuvenation in Pluripotent Cells Reprogrammed via Nuclear Transfer Relative to Induced Pluripotent Stem Cells

Rongrong Le,[1,2] Zhaohui Kou,[2] Yonghua Jiang,[1,2] Ming Li,[2] Bo Huang,[2] Wenqiang Liu,[1,2] Hui Li,[3] Xiaochen Kou,[2] Wanzhong He,[2] Karl Lenhard Rudolph,[4] Zhenyu Ju,[5,*] and Shaorong Gao[2,6,*]
[1]College of Biological Sciences, China Agricultural University, Beijing 100094, China
[2]National Institute of Biological Sciences, NIBS, Beijing 102206, China
[3]Institute of Zoology, Chinese Academy of Sciences, Beijing 100101, China
[4]Leibniz Institute for Age Research, Fritz Lipmann Institute, Jena 07745, Germany
[5]Institute of Aging Research, School of Medicine, Hangzhou Normal University, Hangzhou 310036, China
[6]School of Life Sciences and Technology, Tongji University, Shanghai 200092, China
*Correspondence: zhenyuju@163.com (Z.J.), gaoshaorong@tongji.edu.cn (S.G.)
http://dx.doi.org/10.1016/j.stem.2013.11.005

SUMMARY

Although somatic cell nuclear transfer (SCNT) and induction of pluripotency (to form iPSCs) are both recognized reprogramming methods, there has been relatively little comparative analysis of the resulting pluripotent cells. Here, we examine the capacity of these two reprogramming approaches to rejuvenate telomeres using late-generation telomerase-deficient (*Terc*$^{-/-}$) mice that exhibit telomere dysfunction and premature aging. We found that embryonic stem cells established from *Terc*$^{-/-}$ SCNT embryos (*Terc*$^{-/-}$ ntESCs) have greater differentiation potential and self-renewal capacity than *Terc*$^{-/-}$ iPSCs. Remarkably, SCNT results in extensive telomere lengthening in cloned embryos and improved telomere capping function in the established *Terc*$^{-/-}$ ntESCs. In addition, mitochondrial function is severely impaired in *Terc*$^{-/-}$ iPSCs and their differentiated derivatives but significantly improved in *Terc*$^{-/-}$ ntESCs. Thus, our results suggest that SCNT-mediated reprogramming mitigates telomere dysfunction and mitochondrial defects to a greater extent than iPSC-based reprogramming. Understanding the basis of this differential could help optimize reprogramming strategies.

INTRODUCTION

Telomeres play key roles in maintaining chromosome stability and cell replicative capacity (d'Adda di Fagagna et al., 2003; Hande et al., 1999). Telomere length is primarily maintained by telomerase, a ribonucleoprotein consisting of telomerase transcriptase (TERT) and RNA template (*TERC*) (Greider and Blackburn, 1985, 1987; Yu et al., 1990). During preimplantation development, the telomeres lengthen significantly via a telomerase-independent mechanism known as alternative lengthening of telomeres (ALT), while telomerase activity remains very low. During the transition from the morula to the blastocyst stage, the mechanism of telomere elongation switches from ALT to a telomerase-dependent manner, and the telomere length does not elongate significantly after the blastocyst stage (Liu et al., 2007). Thus, telomere length is thought to be established during the early embryonic stage through the ALT mechanism and to be subsequently maintained by telomerase activity. Progressive telomere shortening due to absent or insufficient telomerase activity can eventually lead to loss of telomere capping function, which plays important roles in driving degenerative pathologies in humans (Sahin and Depinho, 2010).

Induced pluripotent stem cells (iPSCs) hold great promise in future clinical applications, especially in the treatment of degeneration disorders caused by aging. However, the inferior quality of iPSCs, especially derived from patients with premature age-related pathologies, raises significant concerns regarding iPSC safety (Andrade et al., 2012; Batista et al., 2011). Particularly in the context of telomere dysfunction and DNA damage, the resultant activated p53 significantly suppresses nuclear reprogramming, while the absence or mutation of p53 provokes genomic aberrations and tumor formation (Hong et al., 2009; Kawamura et al., 2009; Marión et al., 2009a). Moreover, insufficient telomere lengthening remains a general problem in both human and mouse iPSCs (Marion et al., 2009b; Vaziri et al., 2010). Therefore, telomere elongation during somatic cell reprogramming is of great importance in the acquisition of authentic pluripotency.

It is well accepted that oocytes have the capacity to elongate telomeres via the ALT mechanism (Liu et al., 2007). Indeed, oocyte-derived factor Zscan4 dramatically elongates telomeres during iPSC induction and thus improves the reprogramming efficiency and the quality of iPSCs (Jiang et al., 2013). Furthermore, it has been reported previously that telomeres can be elongated in the cloned animals, even in the case that senescent cells were used as donor cells for SCNT (Lanza et al., 2000; Wakayama et al., 2000). Therefore, we speculate that SCNT utilizing factors in oocytes to reprogram somatic cells may rejuvenate cells with dysfunctional telomeres in a manner superior to that of iPSC technology with only a few reprogramming factors. *Terc*$^{-/-}$ mice provide a model of telomere-driven premature

aging to mimic short telomeres and associated disorders in human premature aging pathologies (Blasco, 2005; Herrera et al., 1999b; Rudolph et al., 1999; Sahin and Depinho, 2010). *Terc*$^{-/-}$ mice can only be bred to four generations in the C57BL/6 background. In the third generation (G3) *Terc*$^{-/-}$ mice, disease states associated with short telomeres become evident, with a reduced body size, a decreased life span, and atrophy of multiple tissues such as small intestine, spleen, and testicles (Herrera et al., 1999b; Rudolph et al., 1999). In these affected tissues, dysfunctional telomeres activate p53-dependent checkpoints and subsequently provoke Puma-dependent cell apoptosis and p21-dependent cell-cycle arrest, causing tissue maintenance disorders (Ferrón et al., 2004; Sperka et al., 2012). Recently, mitochondrial compromise as a consequence of PGC network repression induced by dysfunctional telomeres has been proposed to be another cause for the decline of tissue maintenance in *Terc*$^{-/-}$ mice (Sahin et al., 2011). Based on these studies of the underlying molecular mechanism of telomere-erosion-induced deficiency, we utilized *Terc*$^{-/-}$ mice as a model to compare the differences between SCNT and transcription-factor-mediated reprogramming of cells with limited telomere reserve.

We established embryonic stem cells from *Terc*$^{-/-}$ SCNT embryos (*Terc*$^{-/-}$ ntESCs) and *Terc*$^{-/-}$ iPSCs from G2 and G3 *Terc*$^{-/-}$ somatic cells, respectively. Our study shows that *Terc*$^{-/-}$ ntESCs exhibit a better self-renewal capacity and differentiation potential associated with significantly elongated telomeres and improved mitochondrial function. In contrast, telomere and mitochondrial defects become further impaired in the resulting *Terc*$^{-/-}$ iPSCs and are associated with decreased self-renewal capability and differentiation potential. Interestingly, *PGC-1α* expression appears to be irrelevant to the mitochondrial dysfunction in G3 *Terc*$^{-/-}$ iPSCs. However, failure to reactivate *PGC-1α* expression in differentiating G3 *Terc*$^{-/-}$ iPSCs is associated with an impaired in vitro differentiation ability, which is mitigated in G3 *Terc*$^{-/-}$ ntESCs. Our study suggests that SCNT is superior to iPSCs in reprogramming donor cells with short telomeres and thus provides valuable information for future improvements of iPSCs.

RESULTS

Short Telomeres Decrease Reprogramming Efficiency in the Derivation of Both ntESCs and iPSCs

In the absence of telomerase, telomeres shorten with increasing generations of *Terc*$^{-/-}$ mice (Herrera et al., 1999b; Rudolph et al., 1999). To test the ability of SCNT- and transcription-factor-mediated reprogramming to rejuvenate cells with dysfunctional telomeres, we established ntESCs and iPSCs from tail-tip fibroblasts (TTFs) of aged G2 or G3 *Terc*$^{-/-}$ mice with a pure C57BL/6 genetic background. We transferred the nuclei of G2 or G3 *Terc*$^{-/-}$ TTFs into enucleated oocytes to generate G2 or G3 *Terc*$^{-/-}$ ntESCs. Compared with that of wild-type cloned embryos, the development of *Terc*$^{-/-}$ cloned embryos to morula/blastocyst stage was significantly reduced (Figure 1A). The *Terc*$^{-/-}$ cloned embryos were morphologically normal (Figure 1B). After the blastocysts were plated onto a feeder layer of mouse embryonic fibroblasts, the outgrowths emerged after approximately 5 to 10 days (Figure 1C). *Terc*$^{-/-}$ ntESC lines were derived with significantly lower efficiency compared with wild-type ntESC lines. In total, nine G3 *Terc*$^{-/-}$ ntESC lines were established from 464 cloned embryos (Figure 1A).

With regard to *Terc*$^{-/-}$ iPSCs induction, *Terc*$^{-/-}$ TTFs were infected by doxycyline (Dox)-controlled Tet-on inducible lentiviruses containing Oct4, Sox2, Klf4, and c-Myc transcription factors. The reprogramming kinetics of *Terc*$^{-/-}$ iPSC induction was quite slow. For G3 *Terc*$^{-/-}$ iPSCs, it took at least 25 days of Dox treatment before the ES-like colonies emerged (Figure S1A). Approximately 10–20 colonies emerged from 1×10^5 infected G3 *Terc*$^{-/-}$ fibroblasts, and the reprogramming efficiency (0.019%) was significantly lower than that of wild-type fibroblasts (Figure S1B). In total, 96 colonies were picked and 60 G3 *Terc*$^{-/-}$ iPSC lines were derived from five independent experiments. Hereafter, we designated G2-G3 *Terc*$^{-/-}$ ntESCs and iPSCs as G2-G3 ntESCs and iPSCs, respectively.

Despite the slow kinetics and low reprogramming efficiency, G2-G3 ntESCs and iPSCs showed typical mouse ESC morphology with a compact appearance and a well-defined border (Figure 1D and S1C). Consistent with previous observations, we found that the percentage of cells with a normal karyotype decreased in G3 iPSCs compared with G2 iPSCs (Table S1). In addition, we observed the same tendency toward a decreased frequency of normal karyotype in G3 ntESCs compared with G2 ntESCs (Table S1), indicating that short telomeres exacerbate genomic instability during reprogramming in both iPSCs and ntESCs. We selected cell lines with more than 50% of cells with a normal karyotype for further analysis. Although a relatively low percentage of normal karyotypes was observed in *Terc*$^{-/-}$ ntESCs and iPSCs, *Terc*$^{-/-}$ ntESCs and iPSCs exhibited expression of pluripotent genes at the mRNA and protein levels similar to wild-type (WT) ESCs (Figures 1E and S1D). Furthermore, *Terc*$^{-/-}$ ntESCs and iPSCs showed DNA demethylation at the promoters of *Oct4* and *Nanog*, which are two important transcription factors governing the pluripotent network (Figure 1F).

G3 ntESCs Show Improved Developmental Potential Compared with G3 iPSCs

To evaluate the developmental potential of telomerase-deficient iPSCs and ntESCs, we conducted in vivo and in vitro differentiation assays (Figure 2A). High-contribution chimeric mice could be obtained from G2 ntESCs (Figure 2B and Table S2) while G2 iPSCs, G3 ntESCs, and G3 iPSCs failed to generate viable chimeric mice, which is consistent with a previous report (Marion et al., 2009b). We then examined the developmental potential of G2 iPSCs, G3 ntESCs, and G3 iPSCs by teratoma formation assay. Histological examination revealed that G2 iPSCs and G3 ntESCs could give rise to teratomas containing tissues from three germ layers (Figure 2C). Of notice, none of the 30 G3 iPSC lines with more than 50% of cells with a normal karyotype could generate teratomas (Table S3). Considering that telomere dysfunction may impede cell proliferation rate of G3 iPSCs, we dissected nude mice at different time points after subcutaneous injection of G3 iPSCs and no teratomas were obtained (Table S3). Although G3 iPSCs lost in vivo differentiation ability, under in vitro differentiation conditions the differentiating cells derived from G3 iPSCs showed an upregulation of markers for the three germ layers (Figure 2D). The above data indicated that *Terc*$^{-/-}$ ntESCs showed better differentiation ability than *Terc*$^{-/-}$ iPSCs.

A

Type of donor cells	No. cloned embryos	No. morulae/blastocysts (%)	No. ICM outgrowths	No. ntES cell lines (%)
WT *Terc*$^{+/+}$	178	88(49.44)	50	50(28.09)
G2 *Terc*$^{-/-}$	200	60(30.00)	6	6(3.00)
G3 *Terc*$^{-/-}$	464	104 (22.41)	9	9(1.94)

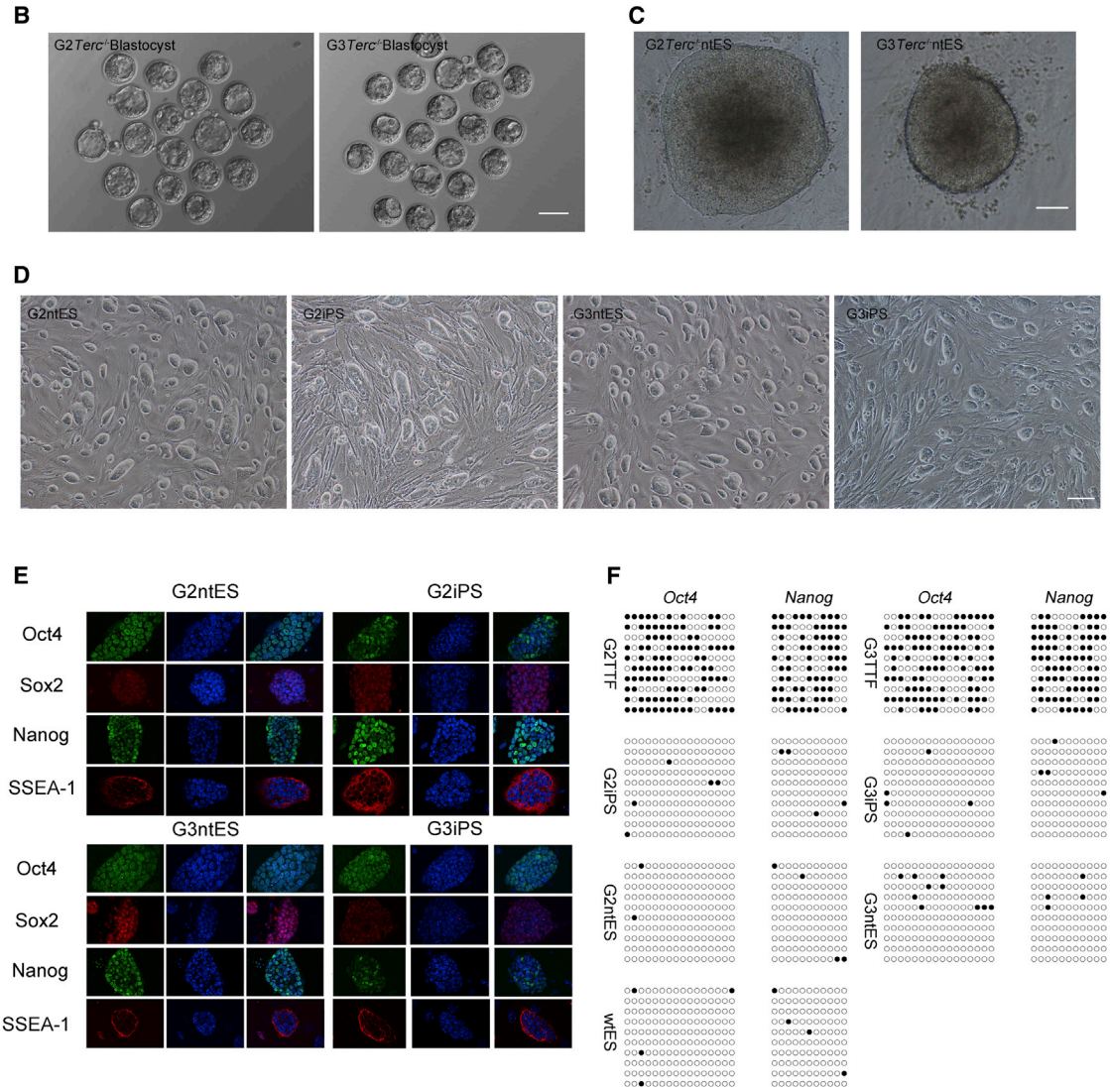

Figure 1. Establishment and Characterization of *Terc*$^{-/-}$ ntESCs and iPSCs from G2-G3 *Terc*$^{-/-}$ Mice

(A) Summary of ntESCs establishment from cloned embryos reconstructed with WT TTFs and *Terc*$^{-/-}$ TTFs. % indicates percentage of reconstructed oocytes. The percentage of cloned embryos that can develop into morulae/blastocysts is markedly decreased in G3 *Terc*$^{-/-}$ cloned embryos compared with WT cloned embryos ($n = 3$; Student's t test; $p < 0.05$). G3 *Terc*$^{-/-}$ ntESC derivation efficiency is significantly decreased compared with WT ntESC derivation efficiency ($n = 3$; Student's t test; $p < 0.005$).

(B) The morphology of *Terc*$^{-/-}$ cloned embryos at the blastocyst stage. Scale bars, 100 μm.

(C) Representative images of the outgrowth morphologies of *Terc*$^{-/-}$ cloned embryos. Scale bars, 40 μm.

(D) Morphology of G2-G3 ntESCs and iPSCs at passage 10. Scale bars, 100 μm.

(E) Immunostaining of pluripotent markers Oct4 (green), Sox2 (red), Nanog (green), and SSEA-1 (red) in G2-G3 ntESC and iPSC lines. Nuclear staining by DAPI (blue).

(F) Bisulfite sequencing shows the methylation state of the promoter regions of *Oct4* and *Nanog*. Open and closed circles indicate unmethylated and methylated CpGs, respectively. For each gene, 10 samples were sequenced, and each line represents one repeat.

See also Figure S1 and Table S1.

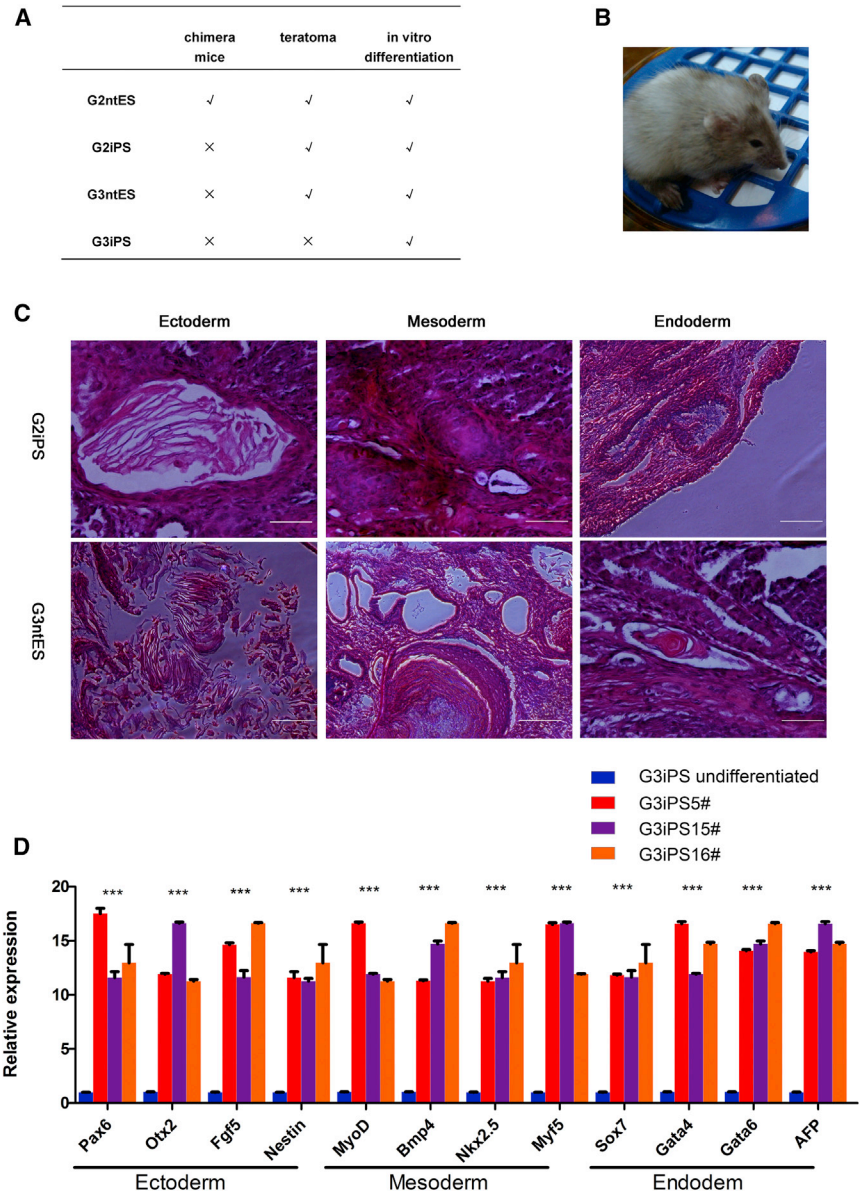

Figure 2. *Terc*$^{-/-}$ ntESCs Show Developmental Potential Superior to That of *Terc*$^{-/-}$ iPSCs

(A) Summary of the differentiation potential of *Terc*$^{-/-}$ ntESCs and iPSCs. See Table S2 and Table S3 for detailed information.

(B) Four-month-old chimeric mice generated from G2 ntES-1#. Cell passage = 5.

(C) H&E staining shows teratomas generated from G2 iPSCs and G3 ntESCs forming tissues from the three germ layers. Upper: G2 iPSCs; lower: G3 ntESCs. Scale bars, 100 μm.

(D) Quantitative PCR analysis shows the upregulation of markers for three germ layers during in vitro differentiation of G3 iPSCs. Relative mRNA expression is normalized to β-actin mRNA and is represented relative to expression in undifferentiated G3 iPSCs as a control, set as 1. The experiments were performed in triplicate (mean ± SD; n = 3; Student's t test; ***$p < 0.001$). The primers used are listed in Table S4.

See also Figure S2, Table S2, Table S3, and Table S4.

It has been reported that a second round of NT makes it possible to clone mice from senescent cells (Mizutani et al., 2008). Based on this finding, we reasoned that a second round of NT from G3 ntESCs might generate 2°-ntESCs with better developmental potential. To this end, we conducted a second round of NT from G3 ntES-2#. Of a total of 242 reconstructed oocytes, 110 developed into morulae/blastocysts, which is more efficient than the first round of NT (Figure S2A). In total, 35 2°-ntESC lines were established. Interestingly, a majority of these cell lines could generate chimeric mice (Figure S2B). In addition, we also generated ntESCs from G3 iPS-5#, G3 iPS-15#, and we named these cell lines G3 iPS-ntESCs. Interestingly, we found that G3 iPS-ntESCs can only be derived from early passage G3 iPSCs (Figure S2A). The differentiation capacity of these cell lines was tested by teratoma formation and contribution of chimeric mice. None of these cell lines could generate chimeric mice (Table S2). In contrast to G3 iPSCs, the G3 iPS-ntESCs could give rise to teratomas with tissues from three germ layers (Figure S2C and Table S3). Collectively, these results demonstrate that the in vivo differentiation defects of G3 *Terc*$^{-/-}$ iPSCs can be rescued by SCNT, which implies that the decreased developmental potential of G3 iPSCs is not caused by the possible existing genetic alterations acquired either from telomerase loss or the process of iPSC induction.

G3 ntESCs Exhibit Increased Proliferation and Reduced Apoptosis Compared with G3 iPSCs

In *Terc*$^{-/-}$ somatic cells, telomere shortening induces both cellular senescence and apoptosis via activation of the p53 signaling pathway, which prompted us to assess the impact of telomere shortening on the proliferation and apoptosis of ntESCs and iPSCs. G3 iPSCs displayed a marked decline in the proliferation rate compared with G2 iPSCs, while the difference between G3 ntESCs and G2 ntESCs was relatively small (Figure 3A and S3A). The BrdU incorporation assay and TUNEL staining revealed significantly reduced proliferation and increased apoptosis levels in G3 iPSCs versus G2 iPSCs and G3 ntESCs versus G2 ntESCs, indicating that progressive telomere shortening induced cell cycle arrest and apoptosis in both iPSCs and ntESCs (Figures S3A and S3B). Notably, G3 ntESCs showed significantly increased proliferation and reduced apoptosis compared with G3 iPSCs (Figures 3A–3C). Interestingly, the difference in proliferative capacity and apoptosis rate was substantially more significant between G3 ntESCs and G3 iPSCs (Figures 3B and 3C) than the

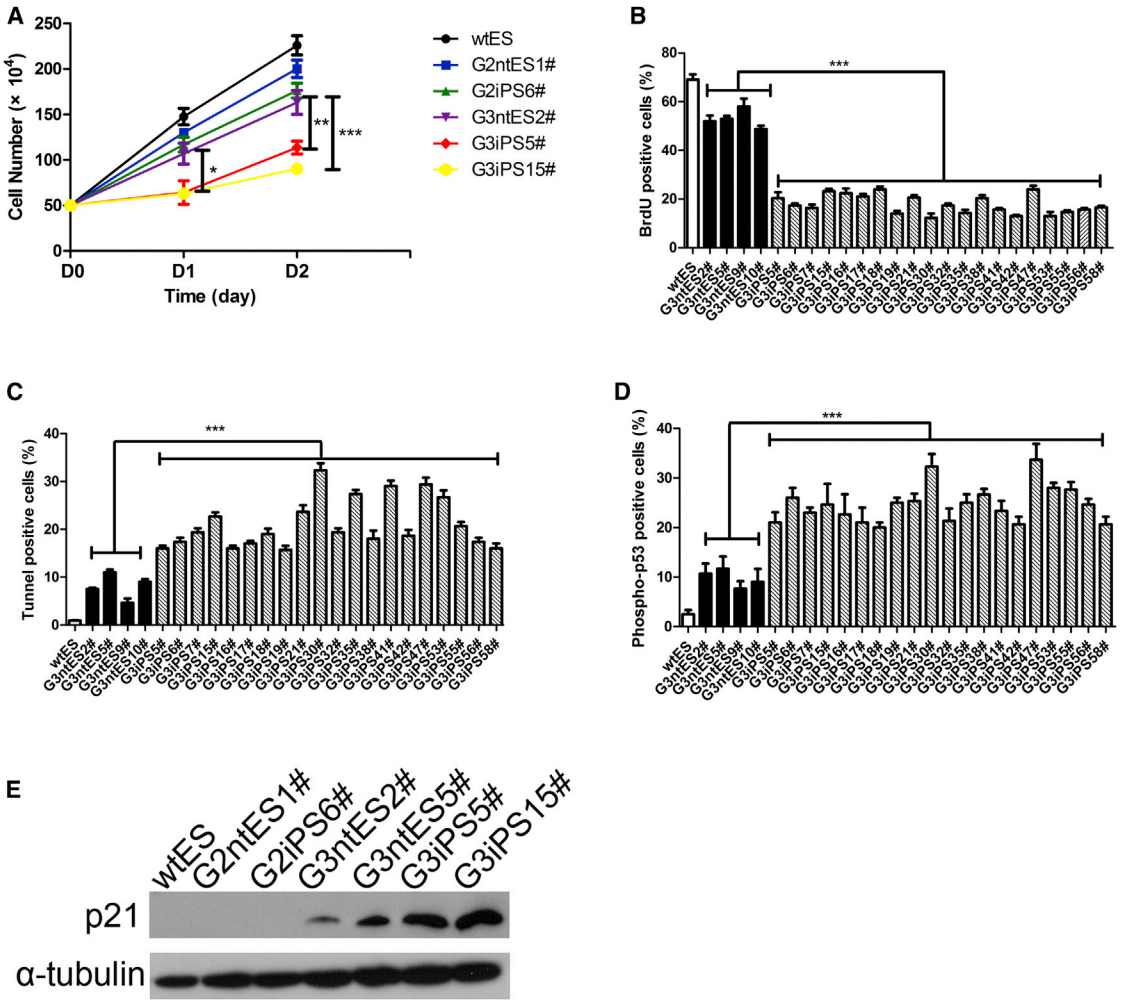

Figure 3. G3 ntESCs Exhibit Increased Proliferation and Reduced Apoptosis Compared with G3 iPSCs

(A) Proliferation curves of G2-G3 ntESCs and iPSCs. A total of 5 × 10^5 cells were seeded in 6-well plates and counted every 24 hr using a cell counting chamber (mean ± SD; n = 3; Student's t test; *p < 0.05, **p < 0.01, ***p < 0.001; cell passage = 10).

(B) Quantification of 5-bromodeoxyuridine (BrdU)-labeled cells by flow cytometry. Cells were cultured in the presence of BrdU for 30 min and then stained with anti-BrdU fluorescent antibodies and subjected to following flow cytometry analysis (mean ± SD; n = 3; Student's t test; ***p < 0.001; cell passage = 10).

(C) Cell apoptosis assay using TUNEL staining and flow cytometry. Cells undergoing apoptosis are positive for TUNEL staining (mean ± SD; n = 3; Student's t test; ***p < 0.001; cell passage = 10).

(D) Quantification of phospho-p53-positive cells using flow cytometry (mean ± SD; n = 3; Student's t test; ***p < 0.001; cell passage = 10).

(E) Western blot analysis of p21 protein levels in G2-G3 ntESCs and iPSCs at passage 15; α-tubulin was used as a loading control.

See also Figure S3.

difference between G2 ntESCs and G2 iPSCs (Figures S3A and S3B), possibly due to a greater level of telomere dysfunction in G3 *Terc*$^{-/-}$ somatic cells. Next, we examined the p53 signaling pathway in G2 or G3 ntESCs and iPSCs. The results showed that the percentage of p53-positive cells increased dramatically in both G2 or G3 iPSCs and ntESCs (Figures 3D and S3C–S3E). Interestingly, the percentage of p53-positive cells in G3 ntESCs was substantially lower than those in G3 iPSCs (Figures 3D, S3D, and S3E). In line with these data, the protein levels of p21, a transcriptional target of p53, increased in both G3 iPSCs and G3 ntESCs, whereas the level of increase was substantially lower in G3 ntESCs compared with G3 iPSCs (Figure 3E).

Telomeres Lengthen Remarkably in *Terc*$^{-/-}$ ntESCs, but Not in *Terc*$^{-/-}$ iPSCs, during Reprogramming

During reprogramming, the average telomere length can be maintained in telomerase-deficient iPSCs, suggesting that a telomerase-independent telomere elongation mechanism exists in iPSC induction (Marion et al., 2009b; Wang et al., 2012). In early cleavage embryos, telomeres lengthen remarkably through a telomerase-independent mechanism (Liu et al., 2007). Thus, it is interesting to assess whether SCNT-based reprogramming could activate a more efficient mechanism to elongate telomeres in the context of telomerase deficiency. To understand the difference between these two reprogramming strategies in resetting telomere length in the absence of telomerase, we analyzed

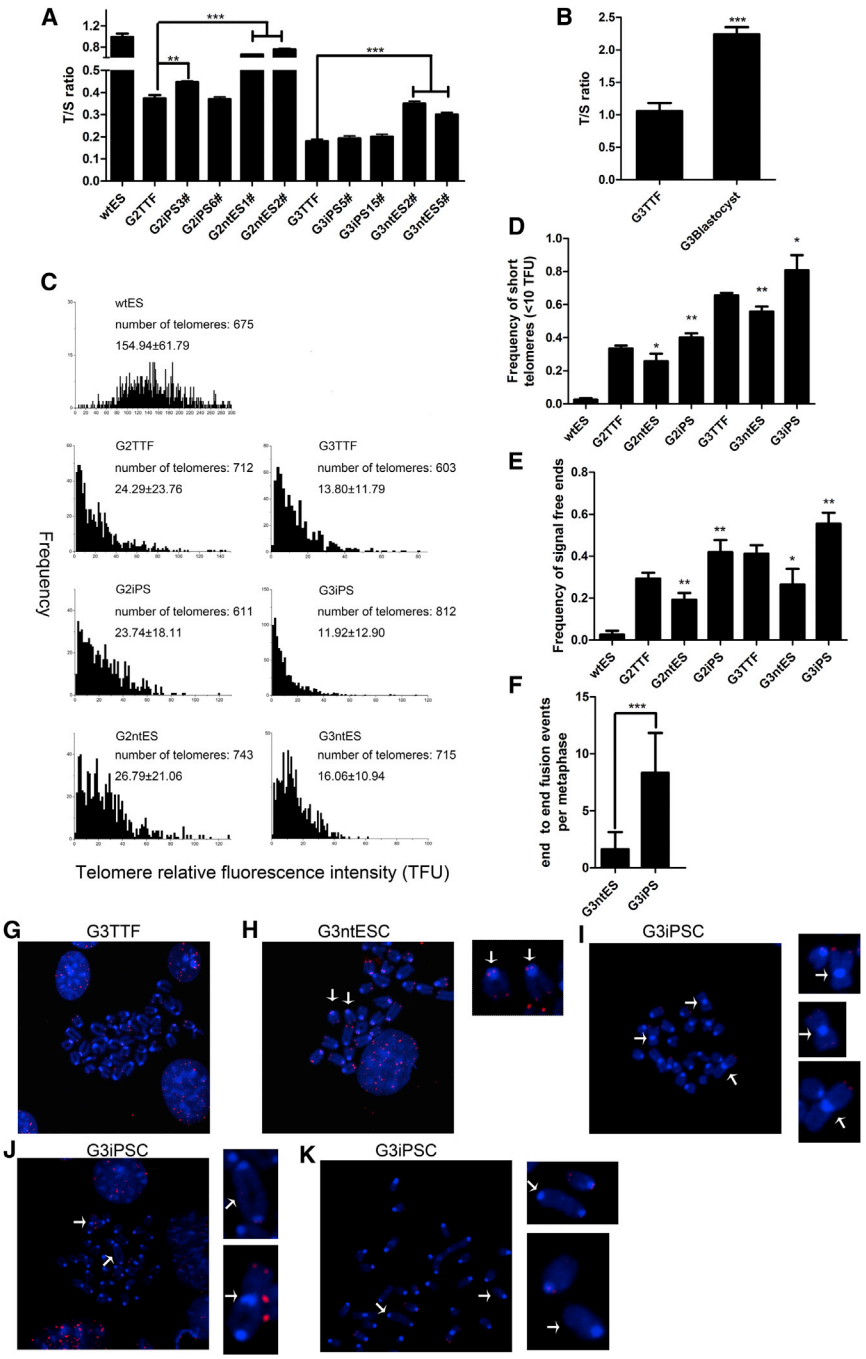

Figure 4. G3 ntESCs Show Improved Telomere Lengthening and Capping Function Compared with G3 iPSCs

(A) Relative telomere length expressed as a T/S ratio by quantitative real-time PCR analysis indicates extensive telomere elongation in *Terc*$^{-/-}$ ntESCs compared with parental TTFs. (mean ± SD; n = 3; Student's t test; **p < 0.01, ***p < 0.001; cell passage = 4).

(B) Relative telomere length expressed as a T/S ratio by quantitative real-time PCR analysis indicates extensive telomere elongation in G3 *Terc*$^{-/-}$ cloned embryos at the blastocyst stage compared with parental somatic cells (mean ± SD; n = 3; Student's t test; ***p < 0.001).

(C) Telomere length distribution shown as relative telomere fluorescence intensity (TFU) by Q-FISH on metaphase spreads. n = 2. Telomere length is shown as the TFU. The average telomere length is shown as the average TFU ± SD. Cell passage = 10.

(D) The frequency of short telomeres by Q-FISH. A total of 30 metaphases per cell type were used (mean ± SD; n = 2; Student's t test; *p < 0.05, **p < 0.01; cell passage = 10).

(E) The frequency of signal free ends by Q-FISH. A total of 30 metaphases per cell type were used (mean ± SD; n = 2; Student's t test; *p < 0.05, **p < 0.01; cell passage = 10).

(F) Quantification of end-to-end fusion events per metaphase of G3 ntESCs and G3 iPSCs (mean ± SD; n = 2, three independent cell lines per cell type and 25 metaphases per cell line in one independent experiment; Student's t test; ***p < 0.001; cell passage = 10).

(G–K) Representative images of metaphase chromosomes after telomere Q-FISH. Telomeres are in red; nuclei labeled by DAPI are in blue. (G) Representative images of G3 TTF metaphase chromosomes. (H) Representative images of G3 ntESCs metaphase chromosomes. The arrows indicate a normal chromosome with four telomere signals. (I) Representative images of G3 iPSC metaphase chromosomes. The arrows indicate p-p arm fusions (right panel). (J) Representative images of G3 iPSC metaphase chromosomes. q-q arm fusions (right panel, top) and p-q arm fusions (right panel, bottom) are shown. (K) Representative images of G3 iPSC metaphase chromosomes. The arrows indicate chromosomes with telomere signal free ends (right panel).

See also Figure S4.

G2-G3 ntESC and iPSC telomeres at early cell passages using q-PCR. The average telomere length as indicated by the T/S ratio elongated dramatically in *Terc*$^{-/-}$ ntESCs while remaining or becoming slightly elongated in *Terc*$^{-/-}$ iPSCs compared with corresponding parental TTFs (Figure 4A). In agreement with this result, a significant increase in telomere length was detected in *Terc*$^{-/-}$ SCNT embryos (Figures 4B and S4A). Overall, these data indicate that the telomerase-independent telomere elongation mechanism is more efficient in SCNT. Of note, telomeres shortened quickly in G3 ntESCs during serial cell passages, reaching a level similar to G3 iPSCs at cell passage 15 (Figure S4B), indicating the requirement of a telomerase-dependent mechanism in the maintenance of telomere length during the passage of pluripotent stem cells.

G3 ntESCs Show Alleviated Telomere Dysfunction Compared with G3 iPSCs

To determine whether telomere dysfunction was improved or worsened in *Terc*$^{-/-}$ ntESCs and iPSCs, quantitative telomere FISH (Q-FISH) on metaphase spreads was performed for a detailed analysis of the telomere distribution pattern within cells (Figures 4C and S4C). The percentage of critically short

telomeres increased in *Terc*$^{-/-}$ iPSCs compared with *Terc*$^{-/-}$ TTFs and was significantly reduced in *Terc*$^{-/-}$ ntESCs (Figures 4C and 4D). Of note, a dramatic shift to critically shorter telomeres was detected in G3 iPSCs (Figures 4C and 4D). In addition, telomere signal free ends indicating telomere uncapping were remarkably decreased in *Terc*$^{-/-}$ ntESCs but dramatically increased in *Terc*$^{-/-}$ iPSCs compared with parental *Terc*$^{-/-}$ TTFs (Figures 4E, 4G, 4H, and 4K). Consistent with the above data, an increase in end-to-end fusion events per metaphase was detected in G3 iPSCs, suggesting an increased level of telomere dysfunction (Figures 4F–4K). These data indicate that although the average telomere length is maintained or even slightly elongated in *Terc*$^{-/-}$ iPSCs, the telomere capping function is further impaired due to an increased frequency of critically short telomeres (Figures 4D and 4E). In contrast, during SCNT-mediated reprogramming, the telomere average length was significantly increased, along with significantly enhanced telomere capping function.

G3 ntESCs Show Alleviated Mitochondrial Dysfunction Compared with G3 iPSCs

To further elucidate the underlying molecular mechanism of the improved pluripotency of G3 ntESCs compared with G3 iPSCs, we performed microarray analyses to profile the transcriptional networks. Cluster analysis showed a marked enrichment of differentially expressed genes related to mitochondria (Figures 5A and S5A), which reminded us of the dysfunctional mitochondria observed in G3 *Terc*$^{-/-}$ somatic cells (Sahin et al., 2011). To assess whether compromised mitochondrial function is improved after somatic cell reprogramming, we analyzed mitochondrial respiration by measuring the rate of oxygen consumption (OCR). The baseline OCR of G3 iPSCs decreased dramatically, while the baseline OCR of G3 ntESCs was comparable to the level in G2 ntESCs and G2 iPSCs (Figures 5B and 5C). FCCP, a compound that uncouples ATP synthesis from the electron transport chain, stimulates the maximum mitochondrial respiration rate. After FCCP injection, a marked increase in OCR was observed in G2 ntESCs, G2 iPSCs, and G3 ntESCs, while G3 iPSCs showed very little increase in OCR (Figures 5B and 5D), suggesting an impaired mitochondrial respiration capacity. Interestingly, the rate of acid efflux (ECAR), indicative of glycolysis activity, also decreased remarkably in G3 iPSCs, whereas G2 ntESCs, G2 iPSCs, and G3 ntESCs displayed levels similar to that of WT ESCs (Figures S5B and S5C). Consistent with the decreased OCR and ECAR levels, the total ATP content was reduced markedly in G3 iPSCs (Figure 5E). During nuclear reprogramming, mitochondrial oxidative metabolism in differentiated cells is transformed into glycolytic metabolism. To assess the relative contribution of glycolysis and mitochondria to the total cellular ATP content, the ATP content was measured in the presence or absence of oligomycin, an inhibitor of ATP synthetase. The proportion of mitochondrial contribution to the total cellular ATP content was markedly elevated in G3 iPSCs, whereas G3 ntESCs showed levels similar to WT ESCs (Figure S5D). In ESCs, mitochondrial energy metabolism was relatively quiescent, accompanied with an immature morphology and poor cristae, while in differentiated cells, mitochondrial energy metabolism was activated and accompanied with an elongated structure and rich cristae. The markedly increased mitochondrial contribution to the total cellular ATP content prompted us to assess mitochondrial morphology in G3 iPSCs and G3 ntESCs. Using cryoelectron microscopy, we observed that the mitochondria in G3 iPSCs were tubular with rich cristae, while the mitochondria in G3 ntESCs were spherical with immature, poor cristae resembling WT ESCs (Figure 5F). Together, the above data suggest that although the mitochondrial respiration capacity is lower in G3 iPSCs, the mitochondria in G3 iPSCs are aberrantly active in energy metabolism, while the mitochondria in G3 ntESCs are quiescent, resembling WT ESCs. These data prompted us to examine the deleterious byproduct of mitochondrial respiration.

Quiescent mitochondria in ESCs can minimize reactive oxygen species (ROS) production and the resulting oxidative stress (Zhang et al., 2012). Of note, we observed sharply increased ROS levels in G3 iPSCs (Figure 5G). Excess ROS accumulation can cause damage to cellular macromolecules. Mitochondrial DNA (mtDNA) is very susceptible to ROS attack, which prompted us to analyze mtDNA mutations in G3 iPSCs. As expected, notable increases in DNA mutations were observed in G3 iPSCs compared with G3 somatic cells and G3 ntESCs, indicating that mtDNA mutations accumulated during the process of transcription-factor-mediated reprogramming and during the subsequent iPSC propagation (Figure 5H). In summary, the above data suggest that unlike the quiescent mitochondrial energy metabolism in G3 ntESCs and WT ESCs, G3 iPSCs exhibit aberrant mitochondrial function with a lower respiration capacity but give rise to ROS overproduction, which, in turn, is associated with an increased mtDNA mutation frequency.

Mitochondrial Dysfunction in G3 iPSCs Is Independent of PGC Network Repression

In *Terc*$^{-/-}$ somatic cells, mitochondrial dysfunction is caused by the telomere-p53-PGC axis (Sahin et al., 2011), which prompted us to analyze the PGC network in G3 iPSCs and ntESCs. Surprisingly, *PGC-1*α and *PGC-1*β were not repressed in G3 ntESCs and iPSCs compared with WT ESCs (Figure 6A). The expression levels of the PGC network's major downstream targets, ERR, TFAM, and NRF-1, in G3 ntESCs and iPSCs were not reduced but were increased compared with WT ESCs (Figure 6B). In addition, mitochondrial DNA content was maintained or even slightly increased in G3 iPSCs and G3 ntESCs (Figure 6C). The above data suggest that mitochondrial dysfunction in G3 iPSCs and G3 ntESCs is independent of PGC network repression.

Next, we questioned whether mitochondrial dysfunction depends on p53 activation. Treating G3 iPSCs with p53 small interfering RNA (siRNA) decreased ROS levels, suggesting that ROS generation partially depends on p53 (Figures S6A and S6B). It is known that p53 can enhance ROS generation enzymes to increase cellular ROS levels. Proline oxidase, a p53 target gene that regulates ROS generation (Donald et al., 2001), was upregulated in G3 iPSCs (Figure S6C). siRNA-mediated knockdown of proline oxidase reduced ROS levels (Figures S6D and S6E), indicating that ROS accumulation in G3 iPSCs partially depends on p53 activation of the ROS-generating enzyme.

Impaired Neuroectoderm Differentiation in G3 iPSCs Is Associated with Mitochondrial Maturation Defect

It has been shown that the increased embryo lethality of *Terc*$^{-/-}$ mice is associated with defects in neuroectodermal

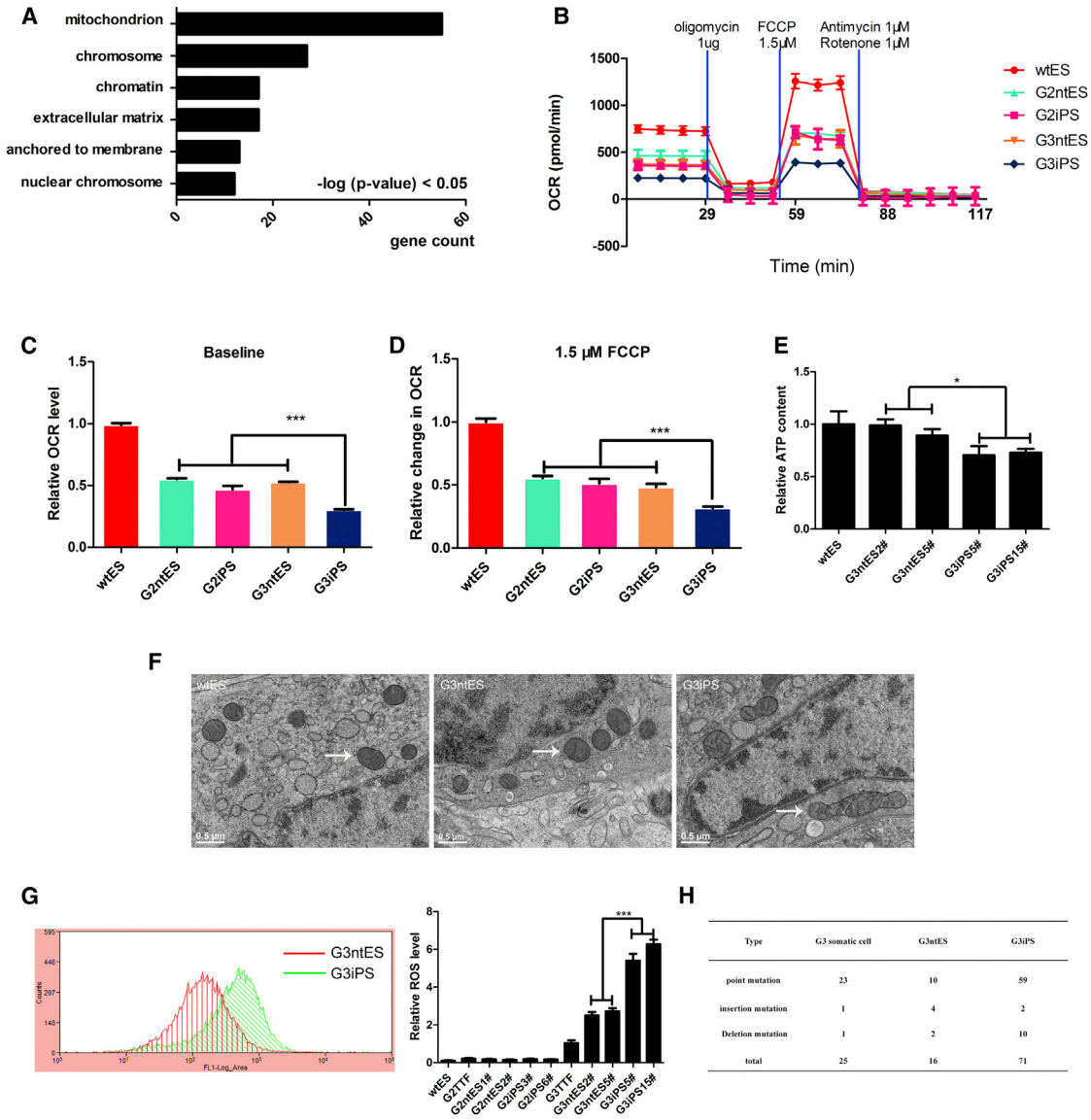

Type	G3 somatic cell	G3ntES	G3iPS
point mutation	23	10	59
insertion mutation	1	4	2
Deletion mutation	1	2	10
total	25	16	71

Figure 5. G3 ntESCs Show Alleviated Mitochondrial Dysfunction Compared with G3 iPSCs

(A) Gene ontology analysis based on cell components of the differentially expressed genes between G3 ntESCs and G3 iPSCs from the microarray data. David Bioinformatics Resources were used to cluster genes from the microarray data. Clustering with $p < 0.05$ was selected.

(B) Oxygen consumption rates (OCRs) in WT ESCs, G2-G3 ntESCs and iPSCs treated sequentially with oligomycin, FCCP, antimycin, and rotenone. (Mean ± SD; n = 3; cell passage = 10.)

(C and D) Basal and maximal OCRs as described in (B). (Mean ± SD; n = 3; Student's t test; ***$p < 0.001$; cell passage = 10.)

(E) Relative ATP content quantification using a luciferin/luciferase-based ATP bioluminescence assay. The ATP content in WT ESCs was set as 1 (mean ± SD; n = 3; Student's t test; *$p < 0.05$; cell passage = 10).

(F) Representative electron microscopy images indicating mitochondrial morphology in WT ESCs, G3 ntESCs and iPSCs. Mitochondria are indicated by arrows (n = 3; cell passage = 10). Scale bars, 0.5 μm.

(G) Left: the ROS levels of G3 ntESCs and G3 iPSCs using flow cytometry. Right: the relative ROS levels in WT ESCs, G2-G3 TTFs, and G2-G3 ntESCs, and iPSCs. The relative ROS level of G3 TTFs is set as 1 (mean ± SD; n = 3; Student's t test; ***$p < 0.001$; cell passage = 10).

(H) Summary of mitochondrial DNA (mtDNA) mutations in G3 ntESCs and iPSCs. mtDNA was divided into six regions, and each region was amplified by PCR. A total of 15 individual sequences for each region were subjected to sequencing. The primers used are listed in Table S4.

See also Figure S5 and Table S4.

differentiation (Herrera et al., 1999a; Lee et al., 1998). In addition, mitochondrial dysfunction has been shown to play a key role in the pathogenesis of many neurodegenerative diseases (Costa and Scorrano, 2012; Exner et al., 2012). To assess the impact of mitochondrial dysfunction on the neuroectodermal differentiation ability of G3 iPSCs and ntESCs, we performed in vitro differentiation oriented to neuronal progenitor cells in the presence of RA using WT ESCs, G3 ntESCs, and G3 iPSCs.

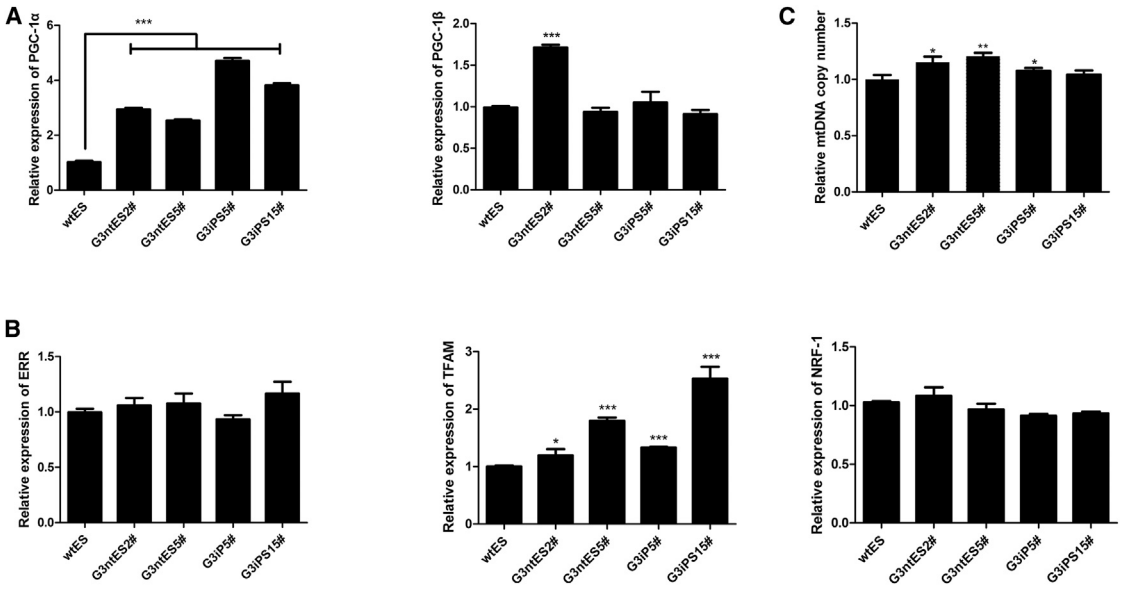

Figure 6. Dysfunctional Mitochondria in G3 iPSCs Are Independent of PGC Network Repression

(A and B) Relative mRNA expression is normalized to β-actin mRNA and is represented relative to expression in WT ESCs as a control, set at 1 (mean ± SD; n = 3; Student's t test; *p < 0.05, ***p < 0.001; cell passage = 15). (A) Quantitative PCR analysis shows upregulation of *PGC-1α* and *PGC-1β* in G3 ntESCs and G3 iPSCs.

(B) Quantitative PCR analysis shows expression of the PGC network's downstream targets in G3 ntESCs and G3 iPSCs.

(C) The relative mtDNA content in G3 ntESCs and G3 iPSCs by quantitative PCR analysis (mean ± SD; n = 3; Student's t test; *p < 0.05, **p < 0.01; cell passage = 15).

See also Figure S6.

EBs derived from G3 iPSCs grew substantially more slowly, and the EB formation ability of G3 iPSCs was markedly reduced compared with that of WT ESCs, whereas these defects were significantly mitigated in G3 ntESCs (Figures 7A and 7B). After plating EBs on PDL/laminin-coated cell culture dishes, we observed cells migrating quickly from adherent EBs derived from WT ESCs and G3 ntESCs and the formation of radial structures with long fibers (Figure S7A). However, we did not observe such transformation of EBs derived from G3 iPSCs. After 5 days of culture under neuron differentiation conditions, neuronal progenitor spheres were generated from WT ESCs and G3 ntESCs, while neuronal progenitor cells failed to arise from G3 iPSCs (Figures 7C and S7B).

During differentiation, mitochondrial biogenesis and maturation through the activation of the PGC network occur for a more efficient energy production, shifting from glycolysis to the mitochondria (Facucho-Oliveira and St John, 2009). To evaluate this process, we harvested cells migrating from EBs under neuron differentiation culture conditions for 5 days. The mitochondrial content notably increased in cells derived from WT ESCs and G3 ntESCs, while no increase was observed in cells derived from G3 iPSCs (Figure 7D). Consistent with these results, *PGC-1α* expression was highly upregulated in WT ESCs and G3 ntESCs, whereas *PGC-1α* expression remained very low in G3 iPSCs (Figure 7E). In addition, the ATP content in cells derived from G3 iPSCs showed a dramatic decrease compared with G3 ntESCs (Figure 7F). In summary, G3 ntESCs display an enhanced neuroectodermal differentiating capability accompanied with alleviated mitochondrial defects and a sufficient reactivation ability of *PGC-1α* compared with G3 iPSCs.

To test whether the *PGC-1α* overexpression could rescue the impaired neuroectodermal differentiation in G3 iPSCs, we established inducible *PGC-1α* overexpression in G3 iPSCs by electroporation delivery of linear pVgRXR and pIND-*PGC-1α* vectors. As shown in Figure 7G, overexpression of *PGC-1α* increased mitochondria content in EBs derived from G3 iPSCs. Accompanied with the mitochondria content increase, EB formation efficiency was also markedly improved (Figure 7H). However, only a small amount of these EBs formed radial structures with long fibers and generated neuron progenitor cells (Figures S7C and 7I). Neuron progenitor cells derived from G3 iPSCs grew very slowly and were passaged every 6–7 days while neuron progenitor cells derived from WT ES and G3 ntESCs were passaged every 3–4 days. The incomplete rescue of the impaired differentiation of G3 iPSCs by *PGC-1α* overexpression suggests other downstream effects of telomerase deficiency or that irreversible mitochondrial damage such as mitochondria mutations may hamper this process. In summary, these data suggest that the mitochondrial biogenesis defect and compromised energy production are associated with the impaired neuroectodermal differentiation capability of G3 iPSCs, which can be partially rescued by *PGC-1α* overexpression.

DISCUSSION

Telomere shortening and mitochondrial dysfunction are closely linked with degenerative pathogenesis in human. Reversion of telomere dysfunction and mitochondrial defects of patients has been considered crucial for the acquisition of authentic pluripotency by somatic cell reprogramming. Here, we utilized somatic

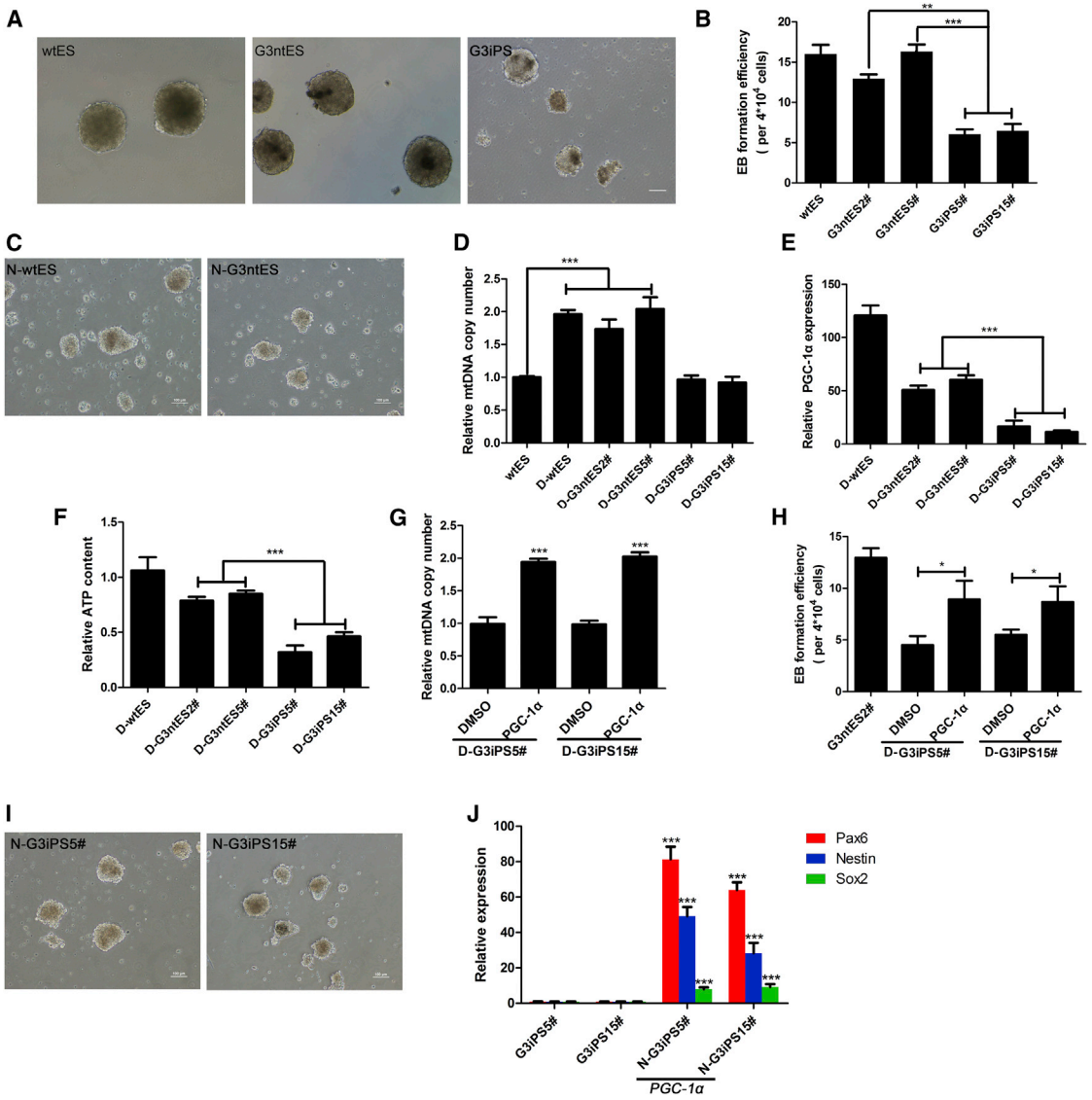

Figure 7. Impaired In Vitro Differentiation Capacity of G3 iPSCs Is Associated with Failure of *PGC-1a* Reactivation

D-wtES, D-G3ntES2#, D-G3ntES5#, D-G3iPS5#, and D-G3iPS15# mean the differentiating cells derived from corresponding parental cells under the neuroectodermal differentiation conditions. N-wtES, N-G3ntES2#, N-G3ntES5#, N-G3iPS5#, and N-G3iPS15# indicate the neuron progenitor cells derived from corresponding parental cells.

(A) Representative images showing EB morphology 4 days after WT ESCs, G3 ntESCs, and G3 iPSCs were subjected to in vitro neuroectodermal differentiation conditions. Scale bar, 100 μm.

(B) EB number (per 4 × 10^4 cells) was calculated 5 days after WT ESCs, G3 ntESCs, and G3 iPSCs were subjected to in vitro neuroectodermal differentiation conditions (mean ± SD; n = 3; Student's t test; **p < 0.01, ***p < 0.001; cell passage = 15).

(C) Images of neuron spheres generated from WT ESCs and G3 ntESCs. Scale bar, 100 μm.

(D) Relative mtDNA content of EBs 5 days after WT ESCs, G3 ntESCs, and G3 iPSCs were subjected to in vitro neuroectodermal differentiation conditions by quantitative PCR analysis (mean ± SD; n = 3; Student's t test; ***p < 0.001; cell passage = 15).

(E) Quantitative PCR analysis shows *PGC1-α* expression in EBs 5 days after WT ESCs, G3 ntESCs, and G3 iPSCs were subjected to in vitro neuroectodermal differentiation conditions. Relative mRNA expression is normalized to β-actin mRNA and is represented relative to expression in undifferentiated WT ESCs as a control, set as 1 (mean ± SD; n = 3; Student's t test; ***p < 0.001; cell passage = 15).

(F) The relative ATP content quantification 10 days after WT ESCs, G3 ntESCs, and G3 iPSCs were subjected to in vitro neuroectodermal differentiation conditions (mean ± SD; n = 3; Student's t test; ***p < 0.001; cell passage = 15).

(G) Relative mtDNA content of EBs 5 days after in vitro neuroectodermal differentiation of G3 iPSCs (mean ± SD; n = 2; Student's t test; ***p < 0.001; cell passage = 15). Overexpression of *PGC-1α* was induced by 10 μM Ponasterone A. Equal volume of Dimethyl sulfoxide (DMSO, 0.1%) was added in the culture as a control (the vehicle in which Ponasterone A is dissolved).

(H) EB number (per 4 × 10^4 cells) was calculated 5 days after in vitro neuroectodermal differentiation of G3 iPSCs (mean ± SD; n = 2; Student's t test; *p < 0.05; cell passage = 15). G3 iPSCs were treated with 10 μM Ponasterone A or equal volume of DMSO (0.1%).

(legend continued on next page)

cells of telomerase-deficient mice as a model to compare the reprogramming competency mediated by SCNT and transcription factors. Interestingly, *Terc*$^{-/-}$ ntESCs show more enhanced differentiation potential and better self-renewal ability than *Terc*$^{-/-}$ iPSCs, and these observations are associated with improved mitochondrial and telomere function.

Telomere elongation is of great importance for the acquisition of pluripotency during reprogramming. Telomere lengthening during iPSC induction mainly relies on telomerase, the action of which is a very time consuming process, and iPSC telomeres need postreprogramming to reach the length resembling that of ESCs (Marion et al., 2009b; Wang et al., 2012). In this study, we have shown that telomeres elongate markedly in cloned embryos reconstructed with telomerase-deficient somatic cells, leading to improved telomere capping function in the established ntESC lines. In contrast, in transcription-factor-mediated reprogramming, telomere function becomes further impaired in the absence of telomerase, although the average telomere length maintains or slightly increases. Our study indicates that the telomerase-independent mechanism is substantially more effective in SCNT than in iPSCs. Elucidating the factors involved in telomere lengthening via the ALT mechanism in SCNT or early embryos might greatly benefit the iPSC induction. This notion is supported by some recent studies on *Zscan4*. This gene specifically marks two cell-embryo and ESCs (Falco et al., 2007; Zalzman et al., 2010). The transient expression of Zscan4 in ESCs is associated with rapid telomere elongation (Zalzman et al., 2010). Addition of Zscan4 in the iPSC induction process efficiently elongates telomeres and enhances the portion of iPSCs with the ability to generate full-term mice (Jiang et al., 2013). It remains elusive if the combination of Zscan4 with Yamanaka factors is sufficient to reprogram somatic cells with limited telomere reserve such as somatic cells of late generation *Terc*$^{-/-}$ mice. Obviously, future studies related to the above question will contribute to the improvement of iPSCs, particularly from patients with telomere or telomerase defects.

Recently, a link between dysfunctional telomeres and impaired mitochondria has been uncovered in somatic and cancer cells (Hu et al., 2012; Sahin et al., 2011). In fact, we observed further mitochondrial impairment in G3 iPSCs, which prompted us to evaluate the association of *PGC-1*α gene expression with mitochondrial quality in our system. Previous studies have shown that the expression level of *PGC-1*β increases as an adaptive mechanism in telomerase-deficient cancer cells to alleviate the mitochondrial dysfunction caused by telomere attrition (Hu et al., 2012). Interestingly, both G3 ntESCs and iPSCs have been shown to upregulate *PGC-1*α and *PGC-1*β expression levels compared with WT ESCs, while dramatic differences in mitochondrial function were still evident between G3 ntESCs and iPSCs. It is plausible that irreversible mitochondrial damage caused by PGC repression may accumulate in the *Terc*$^{-/-}$ somatic cells, which cannot be restored completely simply through an adaptive upregulation of the PGC network. In contrast, the ntESC mitochondria were derived from both somatic cells and recipient oocytes, and the healthier mitochondria from oocytes may improve the overall metabolism competence and lessen the ROS damage. Moreover, telomere attrition is more deleterious in G3 *Terc*$^{-/-}$ iPSCs compared with ntESCs, which may suppress mitochondrial function via a PGC-independent mechanism, as previous work has shown that the effects imposed by p53 activation on mitochondrial function are context dependent (Bae et al., 2005; Matoba et al., 2006). Indeed, we have found that proline oxidase, a p53-targeted ROS generation enzyme, is upregulated in G3 iPSCs and that inhibition of proline oxidase can partially decrease ROS levels, indicating a p53-dependent but PGC-independent network in suppressing G3 iPSC mitochondrial function.

In summary, our study demonstrates that SCNT is superior to transcription factors in reprogramming somatic cells with telomere and mitochondria defects. The breakthrough recently achieved in human SCNT studies further suggests that the identification of novel reprogramming factors might greatly improve the current iPSC technology and enhance the quality of human iPSCs derived particularly from patients with telomere and mitochondria defects (Sancho-Martinez and Izpisua Belmonte, 2013; Tachibana et al., 2013).

EXPERIMENTAL PROCEDURES

Real-Time PCR-Based Quantification of mtDNA Copy Number and mtDNA Sequencing

Total DNA was isolated using Nucleaspin (MACHEREY-NAGEL, Düren, Germany) and then subjected to real-time PCR as previously described (Sahin et al., 2011). For mtDNA sequencing, total DNA was isolated as described above following PCR amplification using primers directed against mtDNA and Phusion High Fidelity PCR Master MIX with HF Buffer (New England Biolabs). The PCR-amplified fragments were cloned into vectors in the pEASYTM-T5 Zero Cloning Kit (TransGen Biotech). mtDNA was divided into six regions for PCR amplification and was subjected to sequencing. For each region, 15 randomly selected clones were sequenced. All primers used are listed in Table S4.

Cell Growth Curve, BrdU Assay, and Apoptosis Analysis

For growth curve analysis, a total of 5 × 10^5 cells were plated onto 35 mm dishes, and the cells were harvested every 24 hr and counted with a cell counting chamber. Each group contained three replicates. For BrdU incorporation assay, pluripotent stem cells were treated with BrdU for 30 min. The cells were stained following the manufacturer's instructions (FITC BrdU Flow Kit, BD). For cell apoptosis detection, 5 × 10^5 pluripotent stem cells were plated onto 35 mm dishes, and 3 days later, the attached cells were harvested using 0.05% trypsin along with the cells in suspension. Staining was performed according to the manufacturer's instructions (DeadEnd™ Fluorometric TUNEL system, Promega). Quantification of BrdU- and TUNEL-positive cells was performed using FACS with standard procedures (Moflo).

Q-FISH and Real-Time-PCR-Based Measurement of Telomere Length

FISH for telomeric DNA was performed with a Cy-3-labeled PNA probe (PANAGENE, Daejeon, Korea) as previously described (Sfeir et al., 2009). For real-time-PCR-based measurement of telomere length, total DNA was extracted from approximately 15 blastocysts or pluripotent stem cells

(I) Images of neuron spheres generated from G3 iPSCs in which *PGC-1*α is overexpressed. Scale bar, 100 μm.
(J) Quantitative PCR analysis shows expression of neuron progenitor cell markers including *Pax6*, *Nestin*, and *Sox2* in the neuron progenitor cells derived from G3 iPSCs (mean ± SD; n = 2; Student's t test; ***p < 0.001; cell passage = 2).
See also Figure S7.

using the QIAamp DNA Micro Kit (QIAGEN). The acidic ribosomal phosphoprotein PO (36B4) gene was used as the endogenous control. The primers and reaction conditions were as previously described (Callicott and Womack, 2006).

OCR and ECAR Measurements Using the Seahorse Cellular Flux Assay

A total of ~5–10 × 10^4 pluripotent stem cells were seeded 24 hr before measurement by the XF24 Seahorse instrument. For bioenergetic profile analysis, oligomycin (1 μg, Sigma), FCCP (1.5 μM, Sigma), and antimycin (1 μM, Sigma) + rotenone (1 μM, Sigma) were sequentially injected into the XF24 assay medium. The XF24 Seahorse instrument was utilized following the manufacturer's instructions, and the reactions were performed in triplicate.

ATP Content and ROS Assay

Total cellular ATP was measured using Mitochondrial ToxGlo (Promega) using an EnSpire Multimode Reader (PerkinElmer). Cellular ROS level was detected with 2,7-dichlorofluorescein diacetate (DCFH-DA, Beyotime).

Electron Microscopy of Cellular Mitochondria

Cultured cells were scraped from dishes and loaded into the 50-μm-deep side of a 50 μm/250 μm aluminum specimen carrier, filled with hexadecene to exclude any air bubble, then sandwiched against the flat side of a 300 μm specimen carrier (Cat.No.390, Cat.No.242 for the two carriers, Engineering Office M. Wohlwend GmbH; Sennwald, Switzerland) and immediately rapid-frozen with HPF Compact 01 high pressure freezing machine (Engineering Office M. Wohlwend GmbH) at 2,100 bar high pressure. The frozen samples were transferred to 1.5 ml microcentrifuge tubes (Fisher Scientific, USA) containing a frozen solution of acetone with 1% OsO_4 and 0.1% uranyl acetate under liquid nitrogen. Tubes were placed in a Leica EM AFS machine (Leica Microsystems, Wetzlar, Germany) at −90°C. The temperature was then gradually raised in 6 hr transitions in the Leica AFS system as follows: −90°C for 24–48 hr, −60°C for 24 hr, and −30°C for 18 hr. After slowly being warmed to 4°C over 2 hr, samples were washed three times in pure acetone and warmed to room temperature. The specimens were infiltrated, embedded, polymerized, sectioned, and stained as previously described (He et al., 2003). We examined 90 nm thin sections using an FEI Tecnai G2 Spirit Twin electron microscope operating at 120 kV, and projection images were recorded on a Gatan 895 4 K × 4 K CCD camera (Gatan Corporation, Pleasanton, CA, USA).

Microarray Analysis

After removal of the feeder cells, total RNA was extracted. The Affymetrix Mouse Gene 1.0 ST Array (Affymetrix, Inc.) was performed at the Beijing CapitalBio Corporation. The multiple tests were adjusted with FDR methods (BH95, R p.adjust command), and a cutoff of FDR $\leq$ 0.05 was chosen as the criterion for significance.

Mice

All of our study procedures were consistent with those in the National Institute of Biological Sciences guide for the care and use of laboratory animals.

Statistical Analysis

Results were represented as the mean ± SD of independent experiments. Significance was determined with Student's t tests using GraphPad Prism software.

ACCESSION NUMBERS

The microarray data sets have been deposited in NCBI's Gene Expression Omnibus (GEO) and are accessible through the GEO accession number GSE46860 (http://www.ncbi.nlm.nih.gov/geo/query/acc.cgi?token=dhylpeuiywsqcxe&acc=GSE46860).

SUPPLEMENTAL INFORMATION

Supplemental Information for this article includes Supplemental Experimental Procedures, seven figures, and four tables and can be found with this article online at http://dx.doi.org/10.1016/j.stem.2013.11.005.

ACKNOWLEDGMENTS

We thank our laboratory colleagues for their assistance with experiments and preparation of the manuscript. We thank Dr. Lin Liu from Nankai University for his thoughtful comments. This work was supported by the Ministry of Science and Technology (2011CB964800, 2012CB911203, 2011CB812700, and 2010CB944900) and the National Natural Science Foundation of China (81130074).

Received: June 10, 2013
Revised: October 3, 2013
Accepted: November 5, 2013
Published: November 21, 2013

REFERENCES

Andrade, L.N., Nathanson, J.L., Yeo, G.W., Menck, C.F., and Muotri, A.R. (2012). Evidence for premature aging due to oxidative stress in iPSCs from Cockayne syndrome. Hum. Mol. Genet. *21*, 3825–3834.

Bae, B.I., Xu, H., Igarashi, S., Fujimuro, M., Agrawal, N., Taya, Y., Hayward, S.D., Moran, T.H., Montell, C., Ross, C.A., et al. (2005). p53 mediates cellular dysfunction and behavioral abnormalities in Huntington's disease. Neuron *47*, 29–41.

Batista, L.F., Pech, M.F., Zhong, F.L., Nguyen, H.N., Xie, K.T., Zaug, A.J., Crary, S.M., Choi, J., Sebastiano, V., Cherry, A., et al. (2011). Telomere shortening and loss of self-renewal in dyskeratosis congenita induced pluripotent stem cells. Nature *474*, 399–402.

Blasco, M.A. (2005). Telomeres and human disease: ageing, cancer and beyond. Nat. Rev. Genet. *6*, 611–622.

Callicott, R.J., and Womack, J.E. (2006). Real-time PCR assay for measurement of mouse telomeres. Comp. Med. *56*, 17–22.

Costa, V., and Scorrano, L. (2012). Shaping the role of mitochondria in the pathogenesis of Huntington's disease. EMBO J. *31*, 1853–1864.

d'Adda di Fagagna, F., Reaper, P.M., Clay-Farrace, L., Fiegler, H., Carr, P., Von Zglinicki, T., Saretzki, G., Carter, N.P., and Jackson, S.P. (2003). A DNA damage checkpoint response in telomere-initiated senescence. Nature *426*, 194–198.

Donald, S.P., Sun, X.Y., Hu, C.A., Yu, J., Mei, J.M., Valle, D., and Phang, J.M. (2001). Proline oxidase, encoded by p53-induced gene-6, catalyzes the generation of proline-dependent reactive oxygen species. Cancer Res. *61*, 1810–1815.

Exner, N., Lutz, A.K., Haass, C., and Winklhofer, K.F. (2012). Mitochondrial dysfunction in Parkinson's disease: molecular mechanisms and pathophysiological consequences. EMBO J. *31*, 3038–3062.

Facucho-Oliveira, J.M., and St John, J.C. (2009). The relationship between pluripotency and mitochondrial DNA proliferation during early embryo development and embryonic stem cell differentiation. Stem Cell Rev. *5*, 140–158.

Falco, G., Lee, S.L., Stanghellini, I., Bassey, U.C., Hamatani, T., and Ko, M.S. (2007). Zscan4: a novel gene expressed exclusively in late 2-cell embryos and embryonic stem cells. Dev. Biol. *307*, 539–550.

Ferrón, S., Mira, H., Franco, S., Cano-Jaimez, M., Bellmunt, E., Ramírez, C., Fariñas, I., and Blasco, M.A. (2004). Telomere shortening and chromosomal instability abrogates proliferation of adult but not embryonic neural stem cells. Development *131*, 4059–4070.

Greider, C.W., and Blackburn, E.H. (1985). Identification of a specific telomere terminal transferase activity in Tetrahymena extracts. Cell *43*, 405–413.

Greider, C.W., and Blackburn, E.H. (1987). The telomere terminal transferase of Tetrahymena is a ribonucleoprotein enzyme with two kinds of primer specificity. Cell *51*, 887–898.

Hande, M.P., Samper, E., Lansdorp, P., and Blasco, M.A. (1999). Telomere length dynamics and chromosomal instability in cells derived from telomerase null mice. J. Cell Biol. *144*, 589–601.

He, W., Cowin, P., and Stokes, D.L. (2003). Untangling desmosomal knots with electron tomography. Science *302*, 109–113.

Herrera, E., Samper, E., and Blasco, M.A. (1999a). Telomere shortening in mTR-/- embryos is associated with failure to close the neural tube. EMBO J. *18*, 1172–1181.

Herrera, E., Samper, E., Martín-Caballero, J., Flores, J.M., Lee, H.W., and Blasco, M.A. (1999b). Disease states associated with telomerase deficiency appear earlier in mice with short telomeres. EMBO J. *18*, 2950–2960.

Hong, H., Takahashi, K., Ichisaka, T., Aoi, T., Kanagawa, O., Nakagawa, M., Okita, K., and Yamanaka, S. (2009). Suppression of induced pluripotent stem cell generation by the p53-p21 pathway. Nature *460*, 1132–1135.

Hu, J., Hwang, S.S., Liesa, M., Gan, B., Sahin, E., Jaskelioff, M., Ding, Z., Ying, H., Boutin, A.T., Zhang, H., et al. (2012). Antitelomerase therapy provokes ALT and mitochondrial adaptive mechanisms in cancer. Cell *148*, 651–663.

Jiang, J., Lv, W., Ye, X., Wang, L., Zhang, M., Yang, H., Okuka, M., Zhou, C., Zhang, X., Liu, L., and Li, J. (2013). Zscan4 promotes genomic stability during reprogramming and dramatically improves the quality of iPS cells as demonstrated by tetraploid complementation. Cell Res. *23*, 92–106.

Kawamura, T., Suzuki, J., Wang, Y.V., Menendez, S., Morera, L.B., Raya, A., Wahl, G.M., and Izpisúa Belmonte, J.C. (2009). Linking the p53 tumour suppressor pathway to somatic cell reprogramming. Nature *460*, 1140–1144.

Lanza, R.P., Cibelli, J.B., Blackwell, C., Cristofalo, V.J., Francis, M.K., Baerlocher, G.M., Mak, J., Schertzer, M., Chavez, E.A., Sawyer, N., et al. (2000). Extension of cell life-span and telomere length in animals cloned from senescent somatic cells. Science *288*, 665–669.

Lee, H.W., Blasco, M.A., Gottlieb, G.J., Horner, J.W., 2nd, Greider, C.W., and DePinho, R.A. (1998). Essential role of mouse telomerase in highly proliferative organs. Nature *392*, 569–574.

Liu, L., Bailey, S.M., Okuka, M., Muñoz, P., Li, C., Zhou, L., Wu, C., Czerwiec, E., Sandler, L., Seyfang, A., et al. (2007). Telomere lengthening early in development. Nat. Cell Biol. *9*, 1436–1441.

Marión, R.M., Strati, K., Li, H., Murga, M., Blanco, R., Ortega, S., Fernandez-Capetillo, O., Serrano, M., and Blasco, M.A. (2009a). A p53-mediated DNA damage response limits reprogramming to ensure iPS cell genomic integrity. Nature *460*, 1149–1153.

Marion, R.M., Strati, K., Li, H., Tejera, A., Schoeftner, S., Ortega, S., Serrano, M., and Blasco, M.A. (2009b). Telomeres acquire embryonic stem cell characteristics in induced pluripotent stem cells. Cell Stem Cell *4*, 141–154.

Matoba, S., Kang, J.G., Patino, W.D., Wragg, A., Boehm, M., Gavrilova, O., Hurley, P.J., Bunz, F., and Hwang, P.M. (2006). p53 regulates mitochondrial respiration. Science *312*, 1650–1653.

Mizutani, E., Ono, T., Li, C., Maki-Suetsugu, R., and Wakayama, T. (2008). Propagation of senescent mice using nuclear transfer embryonic stem cell lines. Genesis *46*, 478–483.

Rudolph, K.L., Chang, S., Lee, H.W., Blasco, M., Gottlieb, G.J., Greider, C., and DePinho, R.A. (1999). Longevity, stress response, and cancer in aging telomerase-deficient mice. Cell *96*, 701–712.

Sahin, E., and Depinho, R.A. (2010). Linking functional decline of telomeres, mitochondria and stem cells during ageing. Nature *464*, 520–528.

Sahin, E., Colla, S., Liesa, M., Moslehi, J., Müller, F.L., Guo, M., Cooper, M., Kotton, D., Fabian, A.J., Walkey, C., et al. (2011). Telomere dysfunction induces metabolic and mitochondrial compromise. Nature *470*, 359–365.

Sancho-Martinez, I., and Izpisua Belmonte, J.C. (2013). Will SCNT-ESCs be better than iPSCs for personalized regenerative medicine? Cell Stem Cell *13*, 141–142.

Sfeir, A., Kosiyatrakul, S.T., Hockemeyer, D., MacRae, S.L., Karlseder, J., Schildkraut, C.L., and de Lange, T. (2009). Mammalian telomeres resemble fragile sites and require TRF1 for efficient replication. Cell *138*, 90–103.

Sperka, T., Song, Z., Morita, Y., Nalapareddy, K., Guachalla, L.M., Lechel, A., Begus-Nahrmann, Y., Burkhalter, M.D., Mach, M., Schlaudraff, F., et al. (2012). Puma and p21 represent cooperating checkpoints limiting self-renewal and chromosomal instability of somatic stem cells in response to telomere dysfunction. Nat. Cell Biol. *14*, 73–79.

Tachibana, M., Amato, P., Sparman, M., Gutierrez, N.M., Tippner-Hedges, R., Ma, H., Kang, E., Fulati, A., Lee, H.S., Sritanaudomchai, H., et al. (2013). Human embryonic stem cells derived by somatic cell nuclear transfer. Cell *153*, 1228–1238.

Vaziri, H., Chapman, K.B., Guigova, A., Teichroeb, J., Lacher, M.D., Sternberg, H., Singec, I., Briggs, L., Wheeler, J., Sampathkumar, J., et al. (2010). Spontaneous reversal of the developmental aging of normal human cells following transcriptional reprogramming. Regen. Med. *5*, 345–363.

Wakayama, T., Shinkai, Y., Tamashiro, K.L., Niida, H., Blanchard, D.C., Blanchard, R.J., Ogura, A., Tanemura, K., Tachibana, M., Perry, A.C., et al. (2000). Cloning of mice to six generations. Nature *407*, 318–319.

Wang, F., Yin, Y., Ye, X., Liu, K., Zhu, H., Wang, L., Chiourea, M., Okuka, M., Ji, G., Dan, J., et al. (2012). Molecular insights into the heterogeneity of telomere reprogramming in induced pluripotent stem cells. Cell Res. *22*, 757–768.

Yu, G.L., Bradley, J.D., Attardi, L.D., and Blackburn, E.H. (1990). In vivo alteration of telomere sequences and senescence caused by mutated Tetrahymena telomerase RNAs. Nature *344*, 126–132.

Zalzman, M., Falco, G., Sharova, L.V., Nishiyama, A., Thomas, M., Lee, S.L., Stagg, C.A., Hoang, H.G., Yang, H.T., Indig, F.E., et al. (2010). Zscan4 regulates telomere elongation and genomic stability in ES cells. Nature *464*, 858–863.

Zhang, J., Nuebel, E., Daley, G.Q., Koehler, C.M., and Teitell, M.A. (2012). Metabolic regulation in pluripotent stem cells during reprogramming and self-renewal. Cell Stem Cell *11*, 589–595.